

New Journal of Chemistry
Supporting Information

Vaporization enthalpy, long-term evaporation and evaporation mechanism of polyethylene glycol-based deep eutectic solvents

Yu Chen^{*a}, Qian Wang^a, Zhenghui Liu^b, Zheng Li^a, Wenjun Chen^c, Liyang Zhou^a, Jiaqing Qin^a, Yaxin Meng^a, Tiancheng Mu^{*c}

¹ Department of Chemistry and Material Science, Langfang Normal University, Langfang 065000, Hebei, P.R. China.

² Department of Chemistry, Taizhou University, Taizhou 318000, Zhejiang, P.R. China.

³ Department of Chemistry, Renmin University of China, Beijing 100872, P.R. China.

* Yu Chen, E-mail: yuchen@iccas.ac.cn; Phone: +86-316-2188211; Fax: +86-316-2112462.

* Tiancheng Mu, E-mail: tcmu@ruc.edu.cn; Phone: +86-10-62514925; Fax: +86-10-62516444.

Contents

Density measurement.....	4
Figure S1. Effect of temperature on the density of PEG-based DESs. All DESs (a), mol ratio by PEG200:NMA (b), mol ratio by PEG200:LA (c), molecular weight (d), composition (e) and HBD (f). The data of density is fitted by the equation of $\rho=aT+b$, where ρ , a , T and b mean density (g cm^{-3}), slope ($\text{g cm}^{-3} \text{ K}^{-1}$), temperature (K) and intercept (g cm^{-3}), respectively.	5
Figure S2. Solubility parameter of PEG-based DESs at 298.15 K in sequence (a) and the investigation of factors affecting solubility parameter, such as mol ratio by PEG200:NMA, mol ratio by PEG200:LA, molecular weight by PEG:thiourea, composition and HBD (b).	6
Table S1. Comparison of $\Delta_f^{\text{g}}H_m^0$ for ionic liquids, organic solvents and DESs in this work at 298.15 K. ^a	7
Figure S3. Mass loss rate dm/dt of DES PEG200:NMA (1:2) at different temperature within the first 60 min.	9
Details for the successful synthesis of PEG-based DESs.....	10
Figure S4. Overlapped comparison of IR spectra for NMA, PEG200 and PEG200:NMA (1:2).	12
Figure S5. IR spectra of NMA as a function of time.	13
Figure S6. Difference IR spectra of NMA as a function of time.	13
Figure S7. IR spectra of PEG200 as a function of time.	14
Figure S8. Difference IR spectra of PEG200 as a function of time.	14
Figure S9. IR spectra of DES PEG200:NMA (1:2) as a function of time.	15
Figure S10. Difference IR spectra of DES PEG200:NMA (1:2) as a function of time.	15
Figure S11. Normalized IR spectra of NMA, PEG200 and DES PEG200:NMA (1:2) at 600 min. The grey- and yellow-colored area is the characteristic peak in PEG200:NMA (1:2) attributed to NMA and PEG200 without the interference with each other, respectively.	16
Figure S12. Band shift of normalized IR spectra for PEG200 or NMA after forming DES PEG200:NMA (1:2) in the wavenumber range of 1340~1200 cm^{-1}	17
Figure S13. Band shift of normalized IR spectra for PEG200 or NMA after forming DES PEG200:NMA (1:2) in the wavenumber range of 1200~800 cm^{-1}	17
Table S2. Cartesian coordinates of all the optimized species by the Gaussian calculation (i.e., output file) for NMA at b3lyp/6-311++g(d, p).	18
Table S3. Cartesian coordinates of all the optimized species by the Gaussian calculation (i.e., output file) for NMA+NMA at b3lyp/6-311++g(d, p).	19
Table S4. Cartesian coordinates of all the optimized species by the Gaussian calculation (i.e., output file) for PEG200 at b3lyp/6-311++g(d, p).	20
Table S5. Cartesian coordinates of all the optimized species by the Gaussian calculation (i.e., output file) for PEG200+PEG200 at b3lyp/6-311++g(d, p).	21
Table S6. Cartesian coordinates of all the optimized species by the Gaussian calculation (i.e., output file) for PEG200:NMA (1:2) at b3lyp/6-311++g(d, p).	23
Figure S14. Charge distribution (a) and bond length with the unit of Å (b) for NAM, PEG200 and PEG200:NMA (1:2) at the level of b3lyp/6-311++g(d, p).	25
Figure S15. Bond length of NMA-NMA.	26
Figure S16. Charge distribution of NMA-NMA.	26
Figure S17. HOMO energy of NMA-NMA.	27

Figure S18. ESP of NMA-NMA.....	27
Figure S19. Bond length of PEG200-PEG200.....	28
Figure S20. Charge distribution of PEG200-PEG200.....	28
Figure S21. LUMO energy of PEG200-PEG200.....	29
Figure S22. ESP of PEG200-PEG200.....	29
Figure S23. Simulated IR spectra of PEG200, NMA and PEG200:NMA (1:2).....	30
Figure S24. Simulated normalized IR spectra of PEG200, NMA and PEG200:NMA (1:2) in the wavenumber range of 3900~3500 cm⁻¹.....	30
Table S7. Simulated IR peak and intensity of PEG200, NMA and PEG200:NMA (1:2).	31
References in Supporting Information:	34

Density measurement

The measured density of water at 298.15 K was 0.99750 g cm⁻³, which was nearly the same as the reported 0.9974[1] or 0.9971 g cm⁻³[2] in the same condition. The maximal uncertainty of the measured density was 0.005%. The value and error bar of the density were displayed with the two-time averaged data and the standard deviation, respectively, by choosing representative DESs PEG200:thiourea (4:1) and PEG400:thiourea (4:1). Density meter should be placed in the glove box for the purpose of totally avoiding the water interference. However, it was very difficult for us to load the density meter into the glove box. Therefore, the following process was adopted for minimizing the effect of moisture on the density of DESs. Namely, during the density-measuring process, the DESs were first extracted with the plastic syringe in the glove box. After the density meter was ready for measurement, plastic syringe loading with DESs were taken outside the glove box to inject DESs into the densimeter nearby immediately. During the above processes, the effect of moisture on the density of DESs could be minimized.

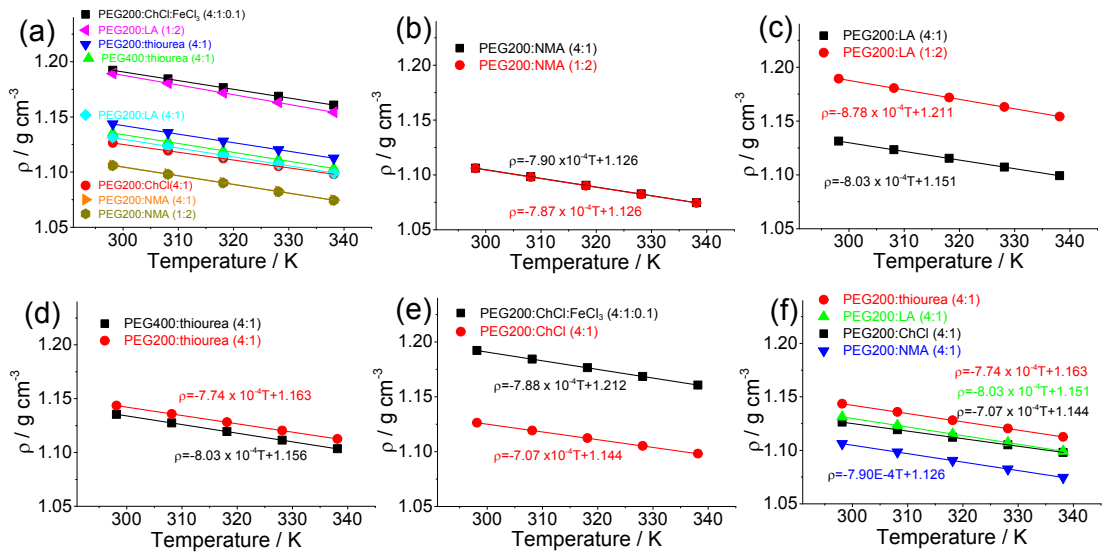


Figure S1. Effect of temperature on the density of PEG-based DESs. All DESs (a), mol ratio by PEG200:NMA (b), mol ratio by PEG200:LA (c), molecular weight (d), composition (e) and HBD (f). The data of density is fitted by the equation of $\rho=aT+b$, where ρ , a , T and b mean density (g cm^{-3}), slope ($\text{g cm}^{-3} \text{ K}^{-1}$), temperature (K) and intercept (g cm^{-3}), respectively.

Discussion on solubility parameter

Hildebrand solubility parameter (δ_H) is the key parameter for estimating solubility, miscibility and intermolecular interaction. The value of δ_H could be determined by vaporization enthalpy, temperature and molar volume (eq S13).[3] Although this parameter is mainly applicable in the situations of nonpolar and slightly polar systems, it gives an important hint of solvation or swelling by seeking systems with similar δ_H .[3, 4] δ_H of PEG-based DESs at 298.15 K (Figure S23) could be ordered as: PEG200:LA (1:2) > PEG200:thiourea (4:1) > PEG200:LA (4:1) > PEG200:ChCl (4:1) > PEG200:NMA (4:1) > PEG400:thiourea (4:1) > PEG200:ChCl:FeCl₃ (4:1:0.1) > PEG200:NMA (1:2). Higher mol ratio of PEG200 increases δ_H in PEG200:NMA but decreases δ_H in PEG200:LA. Also, higher molecular weight (by comparing PEG400:thiourea (4:1) and PEG200:thiourea (4:1)) and presence of FeCl₃ (by comparing PEG200:ChCl:FeCl₃ (4:1:0.1) and PEG200:ChCl (4:1)) would decrease δ_H . However, altering the categories of HBD in PEG-based DESs only slightly changes δ_H . The range of δ_H is from 21.09 to 29.80 MPa^{0.5} for all the PEG-based DESs. Compared with δ_H of common ionic liquids,[3, 5] the value of δ_H for ionic liquids and PEG-based DESs is similar.

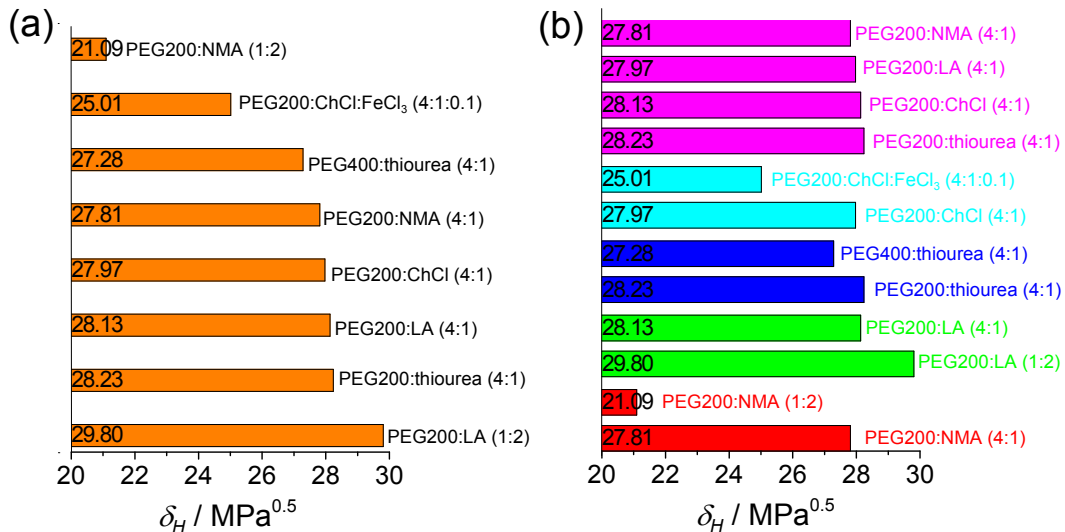


Figure S2. Solubility parameter of PEG-based DESs at 298.15 K in sequence (a) and the investigation of factors affecting solubility parameter, such as mol ratio by PEG200:NMA, mol ratio by PEG200:LA, molecular weight by PEG:thiourea, composition and HBD (b).

Table S1. Comparison of $\Delta_f^{\text{g}}H_m^{\theta}$ for ionic liquids, organic solvents and DESs in this work at 298.15 K.^a

Ionic liquids	$\Delta_f^{\text{g}}H_m^{\theta}$ /kJ mol ⁻¹	Ref.	Organic solvents	$\Delta_f^{\text{g}}H_m^{\theta}$ /kJ mol ⁻¹	Ref.	DESs	$\Delta_f^{\text{g}}H_m^{\theta}$ /kJ mol ⁻¹	Ref.
[C ₁ C ₁ IM][Glu]	238.8	[6]	water	43.98	[3]	PEG200:ChCl (4:1)	133.02	here
[C ₂ C ₁ IM][Glu]	224.1	[6]	methanol	37.43	[3]	PEG200:LA (4:1)	127.03	here
[C ₃ C ₁ IM][Glu]	212.6	[6]	ethanol	42.32	[3]	PEG200:thiourea (4:1)	124.62	here
[C ₄ C ₁ IM][Glu]	203.3	[6]	acetone	30.90	[7]	PEG200:NMA (4:1)	124.55	here
[C ₅ C ₁ IM][Glu]	195.9	[6]	n-pentane	26.7	[7]	PEG400:thiourea (4:1)	117.33	here
[C ₆ C ₁ IM][Glu]	189.8	[6]	n-hexane	31.5	[7]	PEG200:ChCl:FeCl ₃	100.84	here
[H ₂ N-C ₂ C ₁ IM][PF ₆]	165.6	[8]	n-decane	51.4	[7]	PEG200:LA (1:2)	97.13	here
[H ₂ N-C ₃ C ₁ IM][PF ₆]	161.8	[8]	n-dodecane	61.3	[7]	PEG200:NMA (1:2)	87.69	here
[H ₂ N-C ₄ C ₁ IM][PF ₆]	159.2	[8]	n-hexadecane	81.4	[7]			
[H ₂ N-C ₅ C ₁ IM][PF ₆]	157.4	[8]	benzene	33.9	[7]			
[H ₂ N-C ₆ C ₁ IM][PF ₆]	156.4	[8]	dimethylsulfoxide	52.9	NIST			
[MMIM][DMP]	147.02	[3]						
[EMIM][DMP]	142.74	[3]						
[BMIM][DMP]	136.41	[3]						
[EMIM][DEP]	134.23	[3]						
[EEIM][DEP]	134.74	[3]						
[BEIM][DEP]	133.72	[3]						
[BMIM][DBP]	136.11	[3]						
[C ₁ mim][PF ₃ (CF ₂ CF ₃) ₃]	161.9	[9]						
[C ₂ mim][PF ₃ (CF ₂ CF ₃) ₃]	157.8	[9]						
[C ₃ mim][PF ₃ (CF ₂ CF ₃) ₃]	160.3	[9]						
[C ₄ mim][PF ₃ (CF ₂ CF ₃) ₃]	161.1	[9]						
[C ₅ mim][PF ₃ (CF ₂ CF ₃) ₃]	162.0	[9]						
[C ₆ mim][PF ₃ (CF ₂ CF ₃) ₃]	163.1	[9]						
[tmgH][L]	108.0	[10]						
[C ₂ MIM][NTf ₂]	136.1	[11]						
[C ₄ MIM][NTf ₂]	134.6	[11]						
[C ₆ MIM][NTf ₂]	141.6	[11]						
[C ₈ MIM][NTf ₂]	149.0	[11]						
[C ₂ mim][CH ₃ SO ₄]	143.3	[12]						
[C ₂ mim][SCN]	148.7	[12]						
[C ₂ mim][(C ₂ H ₅ O) ₂ PO ₂]	141.9	[12]						
[C ₂ mim][B(CN) ₄]	130.9	[12]						
[C ₂ mim][FAP]	122.5	[12]						
[C ₂ mim][NTf ₂]	132.7	[12]						
[C ₂ mim][CF ₃ SO ₃]	132.8	[12]						
[C ₂ mim][CH ₃ SO ₃]	140.0	[12]						

[MMIM][DMPO ₄]	111.3	[13]						
[EMIM][MeSO ₃]	141.0	[13]						
[EMIM][HSO ₄]	147.0	[13]						
[EMIM][EtSO ₄]	149.0	[13]						
[EMIM][OTS]	169.0	[13]						
[EMIM][CF ₃ SO ₃]	140.0	[13]						
[EMIM][Ntf ₄]	120.0	[13]						
[BMIM][Ntf ₄]	130.0	[13]						
[BMIM][OcSO ₄]	156.0	[13]						
[EMIM][NTf ₂]	121.8	[14]						
[EMIM][C ₂ SO ₄]	155.9	[14]						
[EMIM][C ₁ SO ₄]	149.6	[14]						
[EMIM][SCN]	153.7	[14]						
[EMIM][SCN]	150.2	[14]						
[EMIM][C ₄ SO ₄]	158.4	[14]						
[EMIM][C ₈ SO ₄]	172.0	[14]						
[EMIM][CF ₃ CO ₂]	129.3	[14]						
[EMIM][TFO]	137.9	[14]						
[EMIM][(C ₂ H ₅ O) ₂ PO ₂]	146.1	[14]						
[EMIM][PF ₆]	143.6	[14]						
[EMIM][BF ₄]	135.5	[14]						
[EMIM][B(CN) ₄]	135.6	[14]						
[EMIM][C(CN) ₃]	138.5	[14]						
[EMIM][FAP]	125.8	[14]						
[DBNH][MeCOO]	152.9	[15]						
[DBNH][EtCOO]	159.3	[15]						
[DBNH][nPrCOO]	165.4	[15]						
[DBUH][MeCOO]	178.5	[15]						
[DBUH][EtCOO]	184.9	[15]						
[DBUH][nPrCOO]	190.5	[15]						
[C ₂ Py][Ntf ₄]	131.4	[16]						
[C ₃ Py][Ntf ₄]	134.5	[16]						
[C ₄ Py][Ntf ₄]	138.1	[16]						
[C ₅ Py][Ntf ₄]	141.7	[16]						
[C ₆ Py][Ntf ₄]	145.9	[16]						
[C ₄ C ₄ Im][Br]	166.9	[17]						
[C ₆ C ₆ Im][Br]	177.9	[17]						
[C ₈ C ₈ Im][Br]	181.4	[17]						

^a $\Delta_f H_m^{\theta}$ of DESs is for the first time determined to the best of our knowledge.

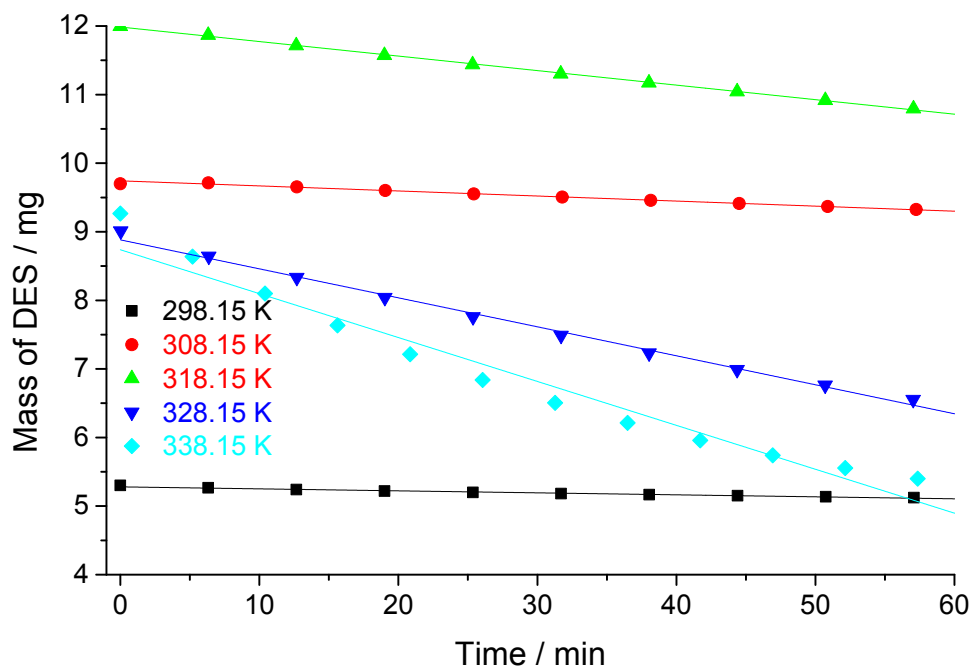


Figure S3. Mass loss rate dm/dt of DES PEG200:NMA (1:2) at different temperature within the first 60 min.

Details for the successful synthesis of PEG-based DESs

Successful synthesis of PEG-based DES could be seen in references.[18-26] Moreover, theoretical and IR spectra provide additional evidences, as shown in Figure 4. There are three possible intermolecular H-bonds between NMA and PEG200, i.e., N-H---O-H (between H of N-H in NMA and O of O-H in PEG200), H-N---O-H (between N of H-N in NMA and O of O-H in PEG200) and C=O---H-O (between O of C=O in NMA and H of H-O in PEG200). H of O-H (in PEG200) and N-H (in NMA) owns a positive charge of +0.253 and +0.170, respectively. O in C=O (in NMA), N of N-H (in NMA) and O of O-H (in PEG200) owns a negative charge of -0.785, -0.728 and -0.639, respectively (Figure 4a). Because O (-0.785) in C=O and H (+0.253) of H-O have the most negative and most positive charge, respectively, H-bonds of C=O---H-O is the optimal mode as shown in Figures 4a, 4b and 4c.

H-bonds between NMA and PEG200 in DES PEG200:NMA (1:2) could also be demonstrated by the bonds length (Figure 4b). Bond length of H-O in PEG200 is 0.961 Å. However, after the formation of DES with NMA, H-O bond length increases into 0.973 Å. Similarly, bond length of C=O in NMA increases from 1.221 Å to 1.229 Å after forming DES. The elongated bond length of H-O in PEG200 and C=O in NMA means the H-bonds (1.878 Å) between NMA and PEG200. However, C-N and C-O, close to the chemical bond forming H-bonds (i.e., C=O and H-O), show a reduced bond length from 1.366 Å to 1.355 Å and from 1.428 Å to 1.419 Å, respectively. It might be induced by the indirect effect of H-bonds. Bond length (1.007 Å) of N-H shows negligible change, indicating that H-bonds related to N-H is not the main H-bonds in DES as discussed above.

HOMO area around O of C=O in NMA and LOMO area around H of H-O in NMA are also the largest, indicating again the high possibility of C=O---H-O H-bonds (Figure 10c). Similarly, C=O---H-O H-bonds is also the highest possible H-bonds from the aspects of electrostatic potential (ESP, Figure 4d). Interaction energy ΔH of PEG200:NMA is also much higher than that of PEG200-PEG200 and NMA-NMA (Figure 4e), implying the strong intermolecular H-bonding interaction between PEG200 and NMA. Moreover, IR spectra of PEG200, NMA and DES PEG200:NMA provide direct evidence of H-bonding interaction between PEG200 and NMA in DES PEG200:NMA as demonstrated by the IR band shift of

PEG200 or NMA after the formation of DES (Table S16, Figure 4f and Supporting Information) .

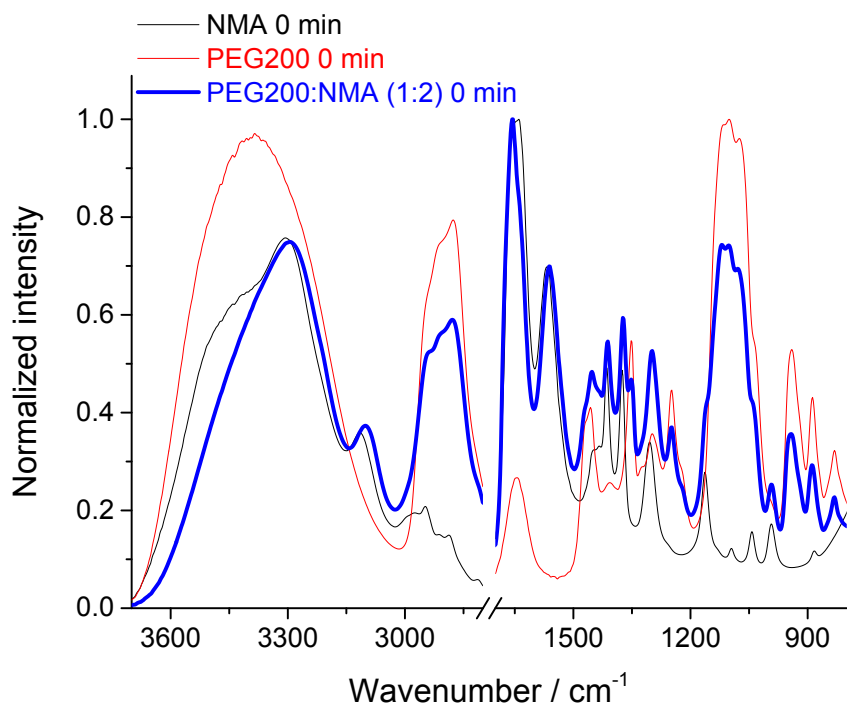


Figure S4. Overlapped comparison of IR spectra for NMA, PEG200 and PEG200:NMA (1:2).

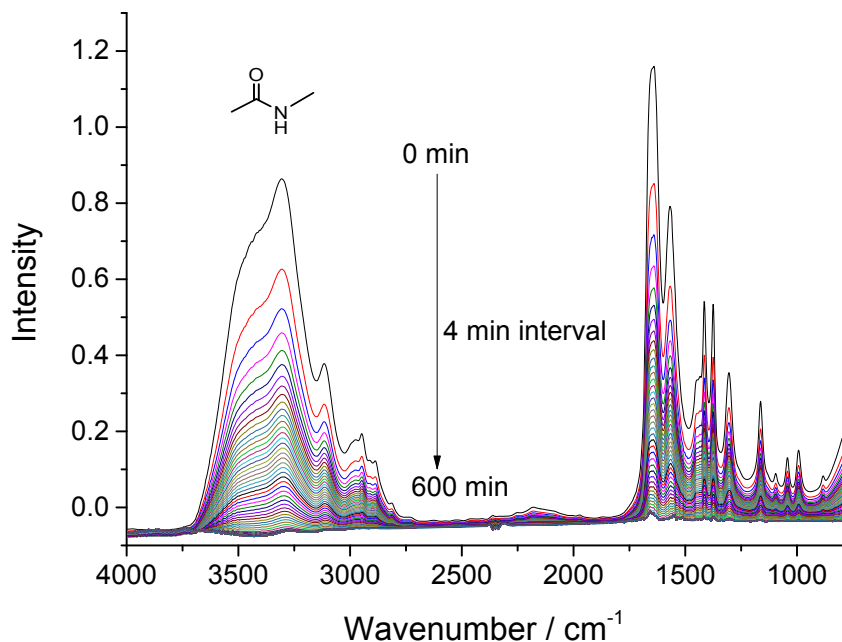


Figure S5. IR spectra of NMA as a function of time.

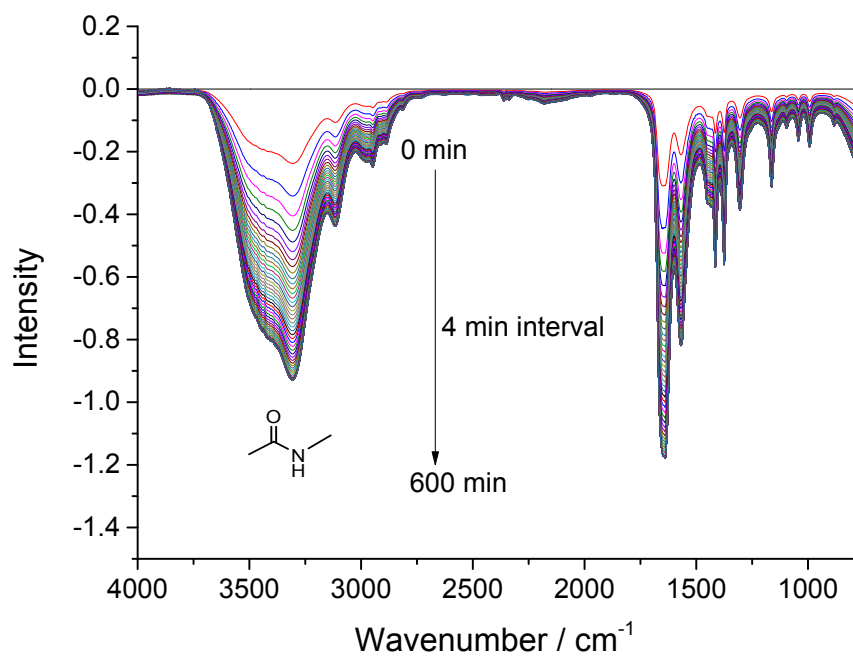


Figure S6. Difference IR spectra of NMA as a function of time.

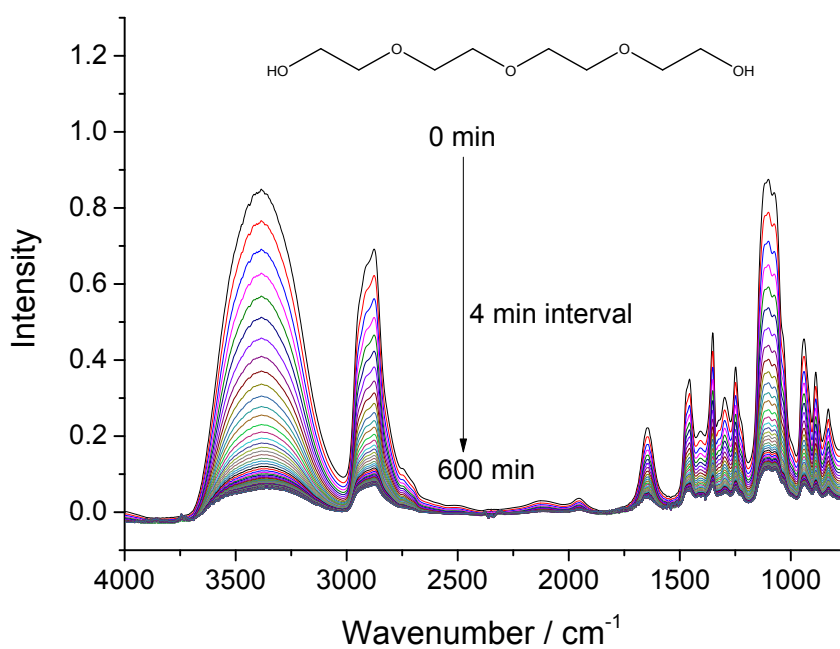


Figure S7. IR spectra of PEG200 as a function of time.

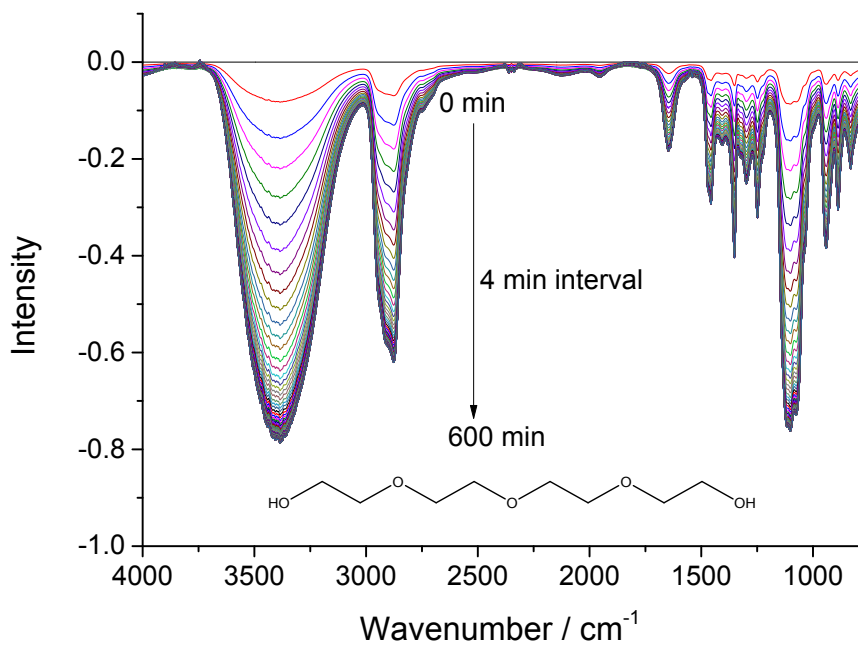


Figure S8. Difference IR spectra of PEG200 as a function of time.

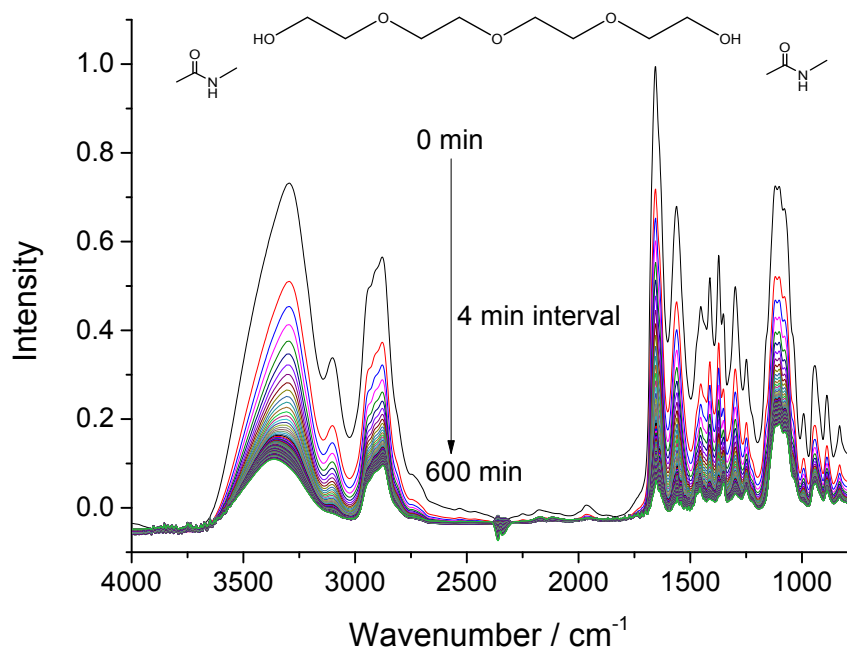


Figure S9. IR spectra of DES PEG200:NMA (1:2) as a function of time.

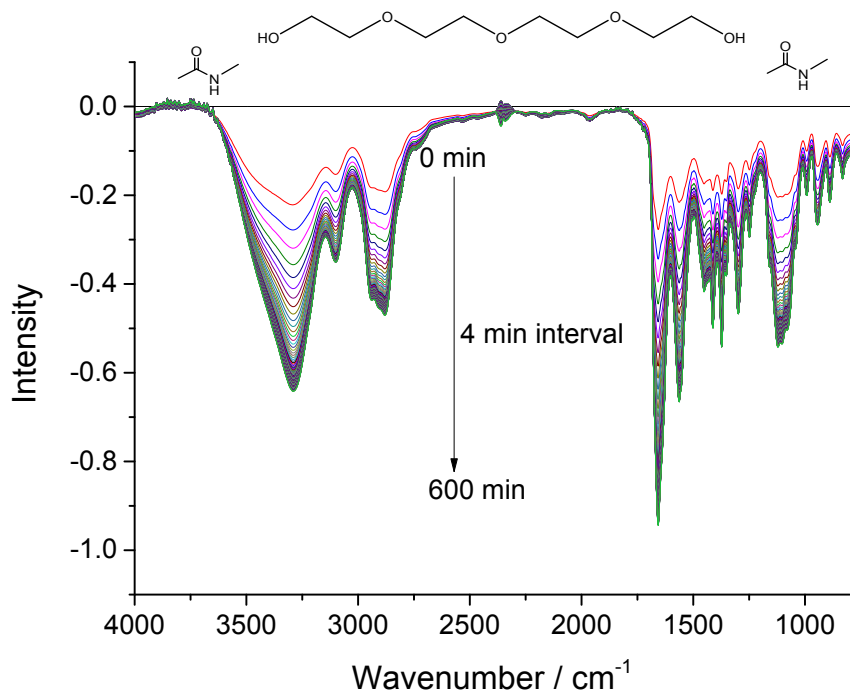


Figure S10. Difference IR spectra of DES PEG200:NMA (1:2) as a function of time.

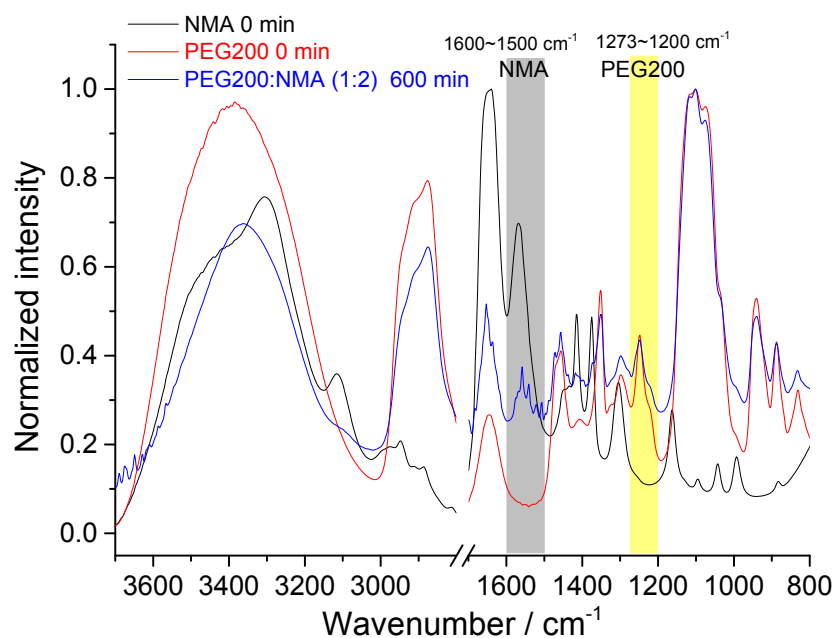


Figure S11. Normalized IR spectra of NMA, PEG200 and DES PEG200:NMA (1:2) at 600 min. The grey- and yellow-colored area is the characteristic peak in PEG200:NMA (1:2) attributed to NMA and PEG200 without the interference with each other, respectively.

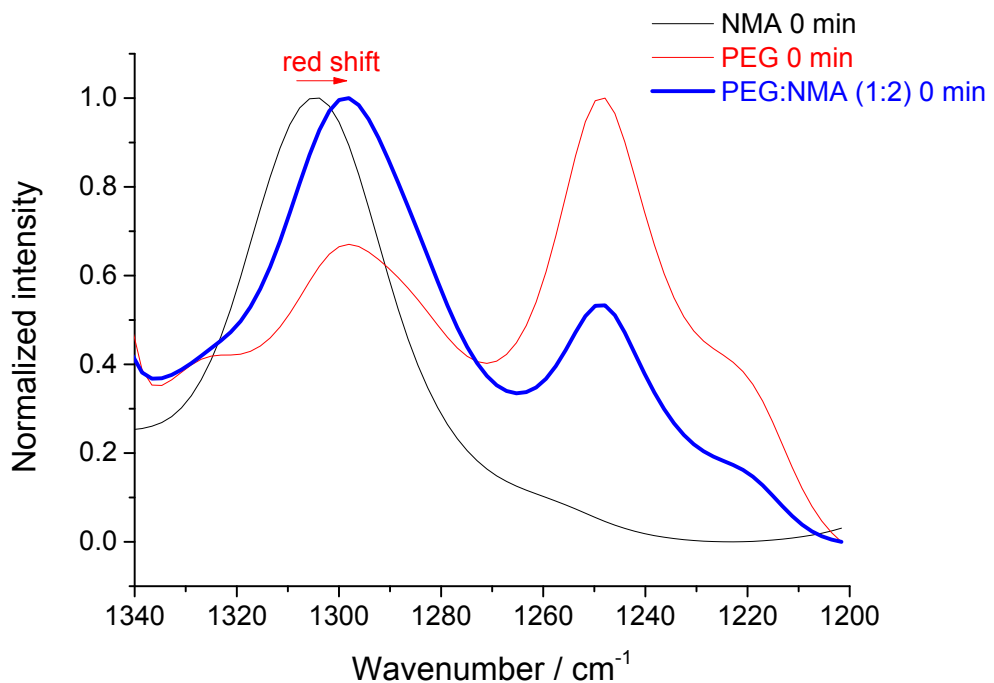


Figure S12. Band shift of normalized IR spectra for PEG200 or NMA after forming DES PEG200:NMA (1:2) in the wavenumber range of 1340~1200 cm⁻¹.

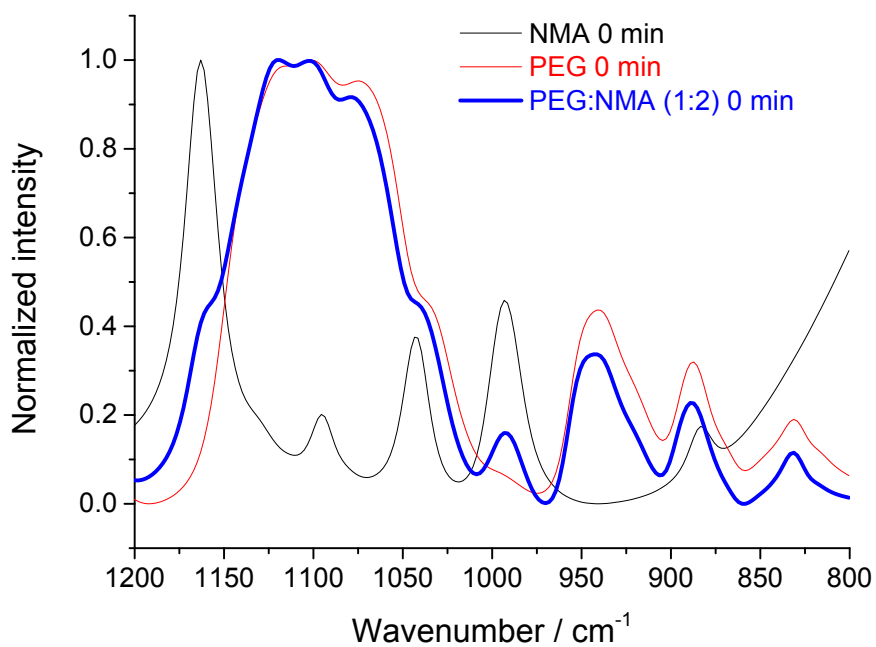


Figure S13. Band shift of normalized IR spectra for PEG200 or NMA after forming DES PEG200:NMA (1:2) in the wavenumber range of 1200~800 cm⁻¹.

Table S2. Cartesian coordinates of all the optimized species by the Gaussian calculation (i.e., output file) for NMA at b3lyp/6-311++g(d, p).

C	0.48613200	0.17262600	0.00002200
O	0.37940300	1.38912900	0.00020200
N	-0.60667500	-0.64613700	-0.00021000
H	-0.47393000	-1.64405000	-0.00004800
C	-1.96119900	-0.11243600	-0.00002400
H	-2.13647000	0.50682600	-0.88295000
H	-2.66623600	-0.94395800	-0.00179900
H	-2.13759300	0.50399200	0.88469000
C	1.83007700	-0.53941100	-0.00000300
H	1.93771600	-1.17319100	0.88494300
H	1.93779000	-1.17300000	-0.88507500
H	2.62016400	0.20862900	0.00011800

Table S3. Cartesian coordinates of all the optimized species by the Gaussian calculation (i.e., output file) for NMA+NMA at b3lyp/6-311++g(d, p).

C	2.69122600	-0.49275900	0.13288800
O	3.90626100	-0.32731300	0.13351500
N	1.82878200	0.41851300	-0.38525500
C	2.31268000	1.64710400	-0.99148100
C	2.05487200	-1.74298100	0.71899200
H	0.82999500	0.24154800	-0.36467900
H	3.00548000	1.43401200	-1.80984500
H	1.45909400	2.20225500	-1.38208300
H	2.84221400	2.26814500	-0.26312900
H	2.47145500	-2.61569600	0.21145800
H	2.33206700	-1.81569800	1.77323400
H	0.96753600	-1.75633000	0.62601300
C	-2.11920900	0.31553400	0.32321800
O	-1.13890400	-0.02744700	-0.33323700
N	-3.37189000	-0.09876500	0.00527100
C	-3.63670900	-1.00041200	-1.10829100
C	-1.99866900	1.23256200	1.52399200
H	-4.13630300	0.17189900	0.60218300
H	-3.46947000	-2.04543300	-0.83064400
H	-4.67129700	-0.87726100	-1.42967100
H	-2.96986000	-0.75513700	-1.93410700
H	-2.95364900	1.44749700	2.00711500
H	-1.32621900	0.77367500	2.25154500
H	-1.54329600	2.17208500	1.20436200

Table S4. Cartesian coordinates of all the optimized species by the Gaussian calculation (i.e., output file) for PEG200 at b3lyp/6-311++g(d, p).

C	1.18420200	0.50021800	0.00037000
C	2.36437600	-0.45671300	0.00015500
H	1.22661600	1.14491300	-0.88864100
H	1.22676900	1.14471200	0.88952000
H	2.32181800	-1.10142200	0.88906200
H	2.32166800	-1.10119600	-0.88890900
C	4.73293500	-0.45560900	-0.00016000
C	5.91415700	0.49915900	-0.00018700
H	4.77662000	-1.10020800	0.88884700
H	4.77633600	-1.09991100	-0.88939500
H	5.86504100	1.13884800	-0.88970700
H	5.86531200	1.13856700	0.88955000
O	3.54808700	0.32222700	0.00015800
O	0.00000000	-0.27810900	0.00038600
O	7.09488700	-0.30321500	-0.00049100
C	-1.18420200	0.50021700	0.00033700
C	-2.36437700	-0.45671400	0.00032100
H	-1.22667800	1.14478700	-0.88876200
H	-1.22670900	1.14483600	0.88939900
H	-2.32161900	-1.10142900	-0.88857200
H	-2.32187000	-1.10119100	0.88939900
C	-4.73293500	-0.45560900	0.00005100
C	-5.91415500	0.49916000	-0.00046400
H	-4.77665800	-1.09979600	0.88935400
H	-4.77629900	-1.10032200	-0.88888800
H	-5.86531500	1.13901100	0.88895500
H	-5.86503900	1.13840400	-0.89030400
O	-3.54808600	0.32222700	0.00005800
O	-7.09488800	-0.30321500	-0.00037400
H	-7.86354200	0.27371100	-0.00074500
H	7.86354200	0.27371000	-0.00058600

Table S5. Cartesian coordinates of all the optimized species by the Gaussian calculation (i.e., output file) for PEG200+PEG200 at b3lyp/6-311++g(d, p).

C	1.18652600	3.06541600	-0.00004200
C	2.35756300	2.09737400	-0.00034700
C	4.72031300	2.05152600	-0.00029400
C	5.92602500	2.97440100	-0.00005900
O	3.55428000	2.85762100	-0.00012400
O	-0.00062800	2.29044900	-0.00023400
O	7.08756200	2.14038400	-0.00019400
C	-1.18781600	3.06536300	0.00003200
C	-2.35881900	2.09727800	-0.00017900
C	-4.72157800	2.05140100	0.00001000
C	-5.92730400	2.97426000	0.00030700
O	-3.55555400	2.85750100	0.00010600
O	-7.08881800	2.14021700	0.00020200
H	1.23150600	3.70977100	-0.88916100
H	1.23155300	3.70925600	0.88944800
H	2.30792000	1.45213700	0.88726400
H	2.30790900	1.45267500	-0.88834900
H	4.74566400	1.40491700	0.88754600
H	4.74569200	1.40533100	-0.88843600
H	5.89665400	3.61485400	-0.88961900
H	5.89659000	3.61447900	0.88976900
H	-1.23288700	3.70970500	-0.88909200
H	-1.23280800	3.70921200	0.88951700
H	-2.30920600	1.45256300	-0.88817200
H	-2.30910300	1.45206000	0.88744100
H	-4.74688200	1.40479700	0.88785700
H	-4.74701600	1.40519900	-0.88812700
H	-5.89784400	3.61432300	0.89014500
H	-5.89797500	3.61472800	-0.88924400
H	-7.87057700	2.69941700	0.00043600
C	1.18046300	-2.08292700	0.00030700
C	2.37533900	-3.02102000	0.00014000
C	4.74888000	-2.95853900	0.00014200
C	5.89785500	-1.96520800	0.00028900
O	3.54121800	-2.21464400	0.00028600
O	0.00068500	-2.86860600	0.00012200
O	7.10782400	-2.72222000	0.00018700
C	-1.17932000	-2.08326200	0.00019200
C	-2.37392000	-3.02170600	-0.00002000

C	-4.74747800	-2.95993100	-0.00017300
C	-5.89674600	-1.96693700	-0.00026800
O	-3.54003900	-2.21567600	-0.00004400
O	-7.10649300	-2.72430000	-0.00034900
H	1.21521400	-1.43652600	-0.88748700
H	1.21517300	-1.43688400	0.88836400
H	2.34695000	-3.66628900	0.88922600
H	2.34694600	-3.66596400	-0.88918100
H	4.81048600	-3.60146700	0.88928900
H	4.81045600	-3.60117000	-0.88922100
H	5.82869800	-1.32637200	-0.88788500
H	5.82868800	-1.32662700	0.88864600
H	-1.21419400	-1.43690800	-0.88763100
H	-1.21427700	-1.43719100	0.88821800
H	-2.34525300	-3.66670700	-0.88929000
H	-2.34542500	-3.66690100	0.88911600
H	-4.80896800	-3.60274200	0.88906500
H	-4.80879500	-3.60271300	-0.88944500
H	-5.82782300	-1.32820100	0.88799800
H	-5.82769400	-1.32822100	-0.88853900
H	-7.84897400	-2.11359800	-0.00039600
H	7.85012000	-2.11129200	0.00013700
H	7.86930300	2.69960900	-0.00009000

Table S6. Cartesian coordinates of all the optimized species by the Gaussian calculation (i.e., output file) for PEG200:NMA (1:2) at b3lyp/6-311++g(d, p).

C	-2.36704700	-0.68979600	0.05643100
C	-1.18425600	0.26210800	0.11947900
C	1.18422300	0.26206200	0.11952900
C	2.36697900	-0.68989900	0.05672600
C	4.73546600	-0.68821200	0.05679300
C	5.92522700	0.25455900	0.12089000
O	-0.00003100	-0.51500200	0.06768600
O	-3.54802000	0.08781500	0.10764800
O	3.54797900	0.08768800	0.10765900
O	7.09907600	-0.54104100	0.06432800
C	-4.73553100	-0.68802400	0.05650200
C	-5.92525900	0.25477500	0.12081000
O	-7.09913600	-0.54077600	0.06407500
H	-2.32423300	-1.39269900	0.90071200
H	-2.32398400	-1.27550200	-0.87301100
H	-1.22603600	0.96457300	-0.72473700
H	-1.22577800	0.84677000	1.04916300
H	1.22614600	0.96442100	-0.72476800
H	1.22564600	0.84683700	1.04914600
H	2.32419300	-1.39255200	0.90121600
H	2.32384300	-1.27587900	-0.87254000
H	4.77370600	-1.39182100	0.90064600
H	4.77520700	-1.27295000	-0.87342300
H	5.87426700	0.95894900	-0.71978600
H	5.87660400	0.83552100	1.05115200
H	7.87889900	0.03869300	0.11048000
H	-4.77384800	-1.39187000	0.90015500
H	-4.77524500	-1.27249800	-0.87388100

H	-5.87661200	0.83552700	1.05120000
H	-5.87428900	0.95934500	-0.71971300
H	-7.87894300	0.03895000	0.11054300
C	10.64222400	0.81813600	-0.08680500
O	9.44757300	1.03374900	0.10609700
N	11.14028300	-0.43355500	-0.23514100
C	10.30489100	-1.62774600	-0.14993000
C	11.63821300	1.95703200	-0.17407600
H	12.13237500	-0.54434500	-0.36374600
H	9.45600700	-1.55403300	-0.83050200
H	10.90836000	-2.49317700	-0.42270000
H	9.91516300	-1.76698900	0.86128600
H	11.32748000	2.63157000	-0.97423600
H	11.60708400	2.52040500	0.76069000
H	12.66290200	1.62952200	-0.36025400
C	-10.64223000	0.81806400	-0.08701700
O	-9.44777500	1.03397300	0.10677000
N	-11.14003600	-0.43380200	-0.23470000
C	-10.30458800	-1.62783900	-0.14787700
C	-11.63826400	1.95678300	-0.17614800
H	-12.13196900	-0.54478200	-0.36436000
H	-9.91437300	-1.76526500	0.86338800
H	-10.90822100	-2.49374100	-0.41878300
H	-9.45602800	-1.55539600	-0.82900800
H	-11.60799800	2.52098200	0.75814800
H	-11.32690900	2.63064700	-0.97663400
H	-12.66275900	1.62900500	-0.36291600

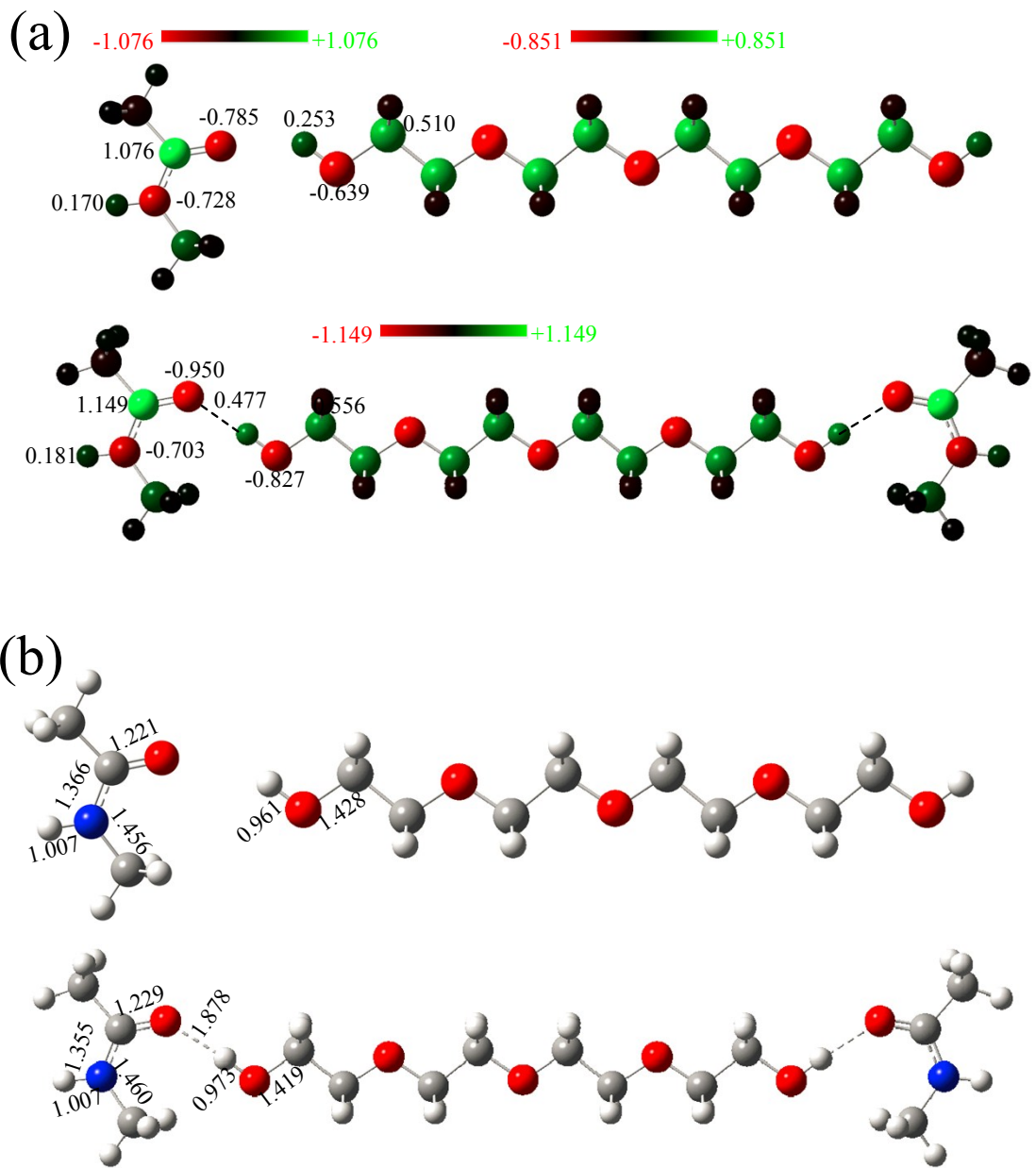


Figure S14. Charge distribution (a) and bond length with the unit of Å (b) for NAM, PEG200 and PEG200:NMA (1:2) at the level of b3lyp/6-311++g(d, p).

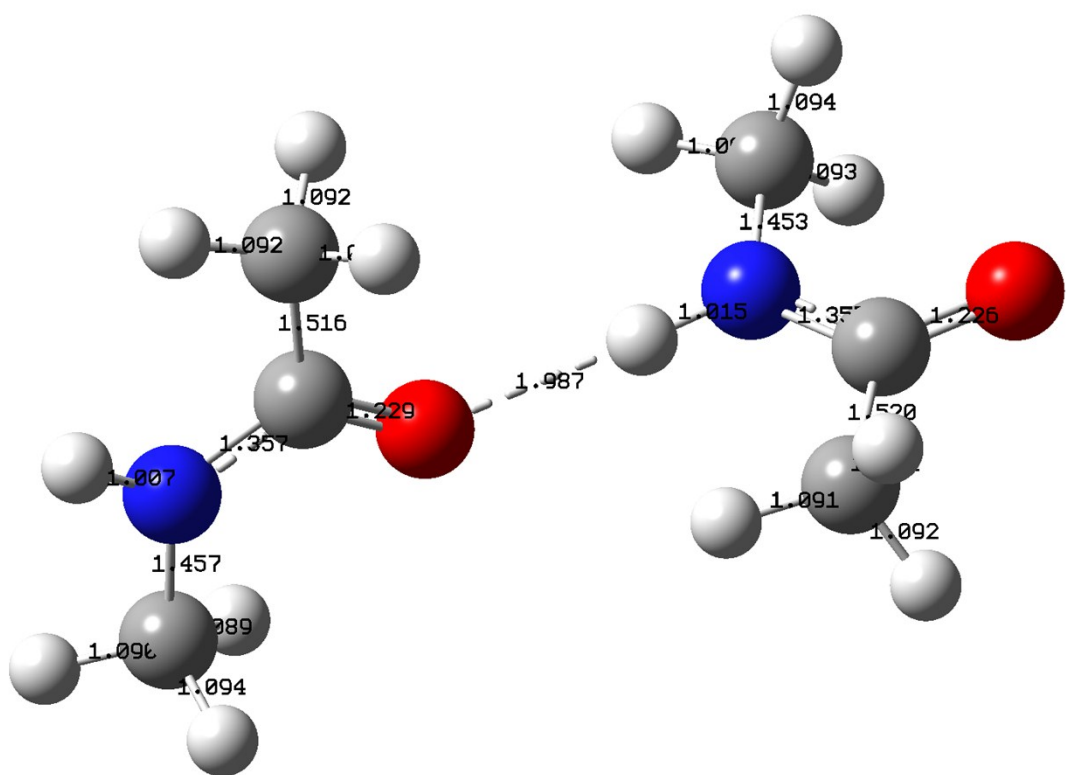


Figure S15. Bond length of NMA-NMA.

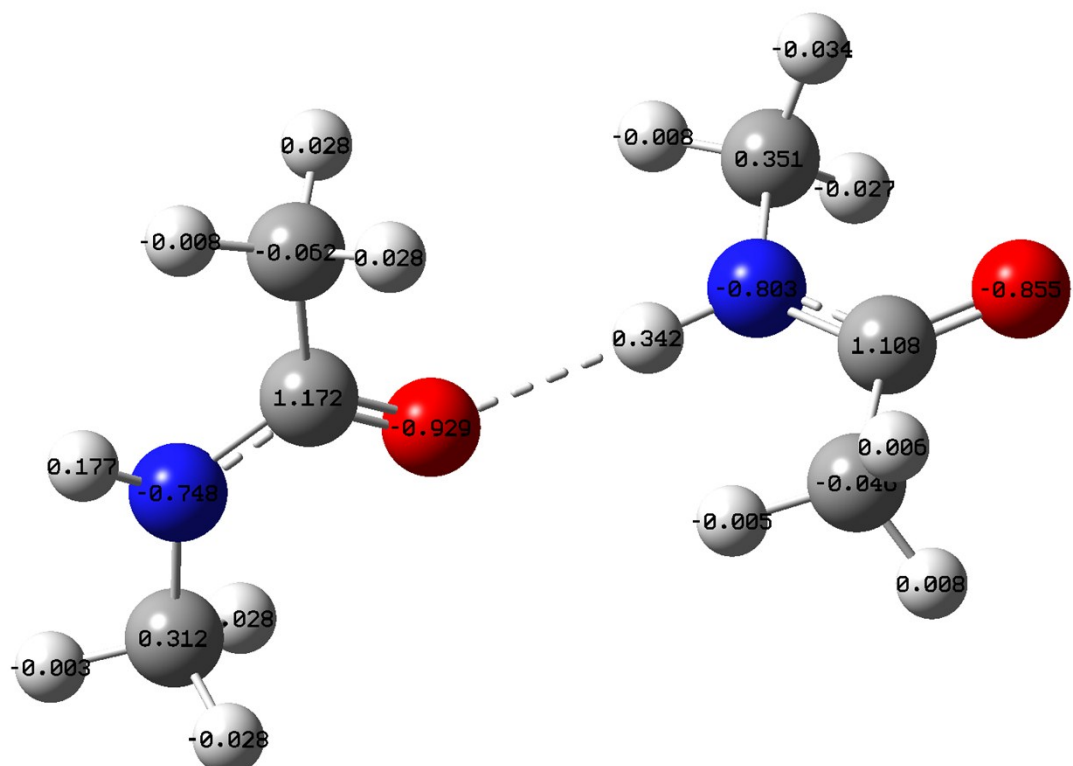


Figure S16. Charge distribution of NMA-NMA.

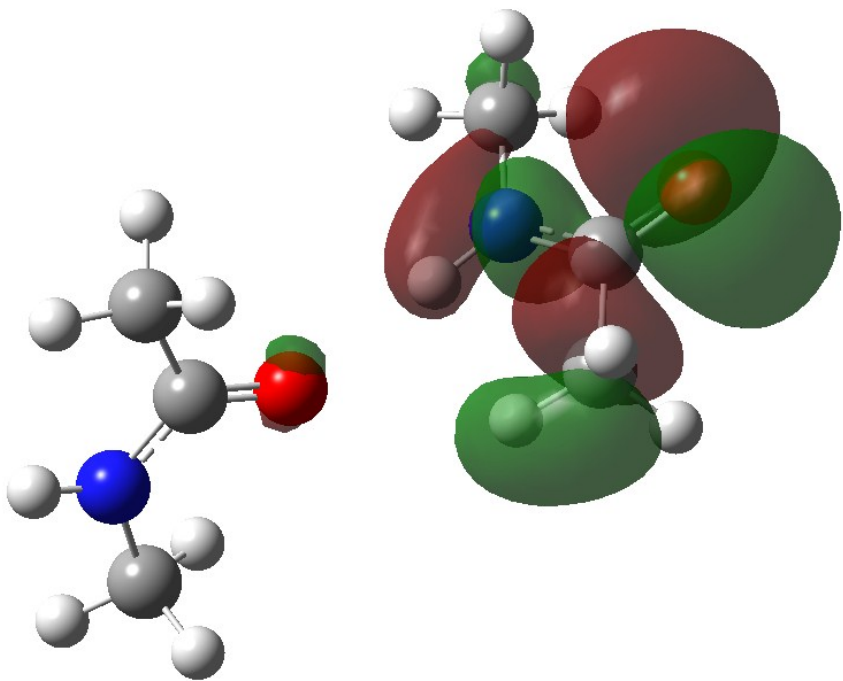


Figure S17. HOMO energy of NMA-NMA.

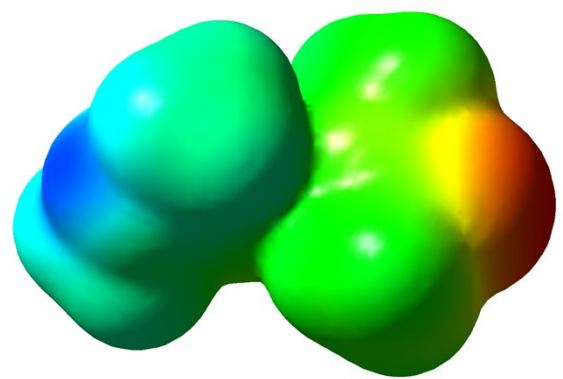


Figure S18. ESP of NMA-NMA.

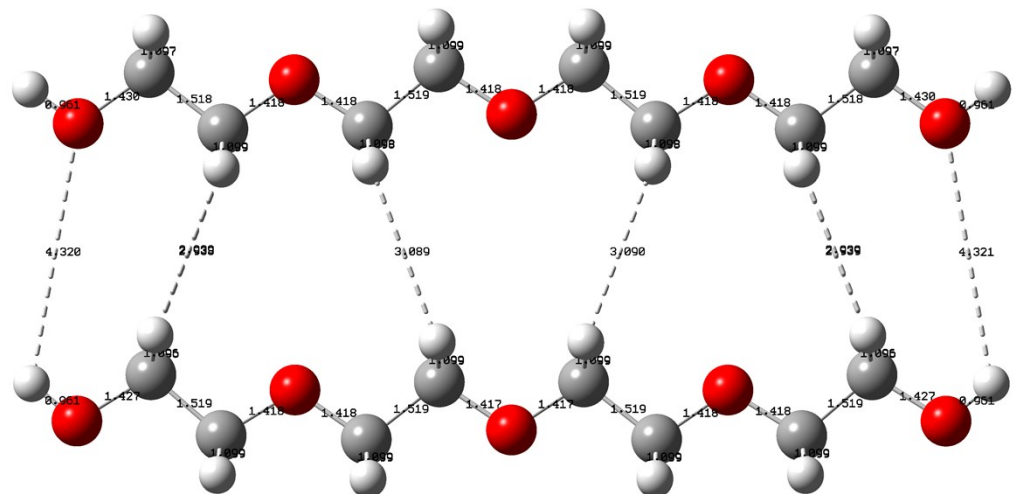


Figure S19. Bond length of PEG200-PEG200.

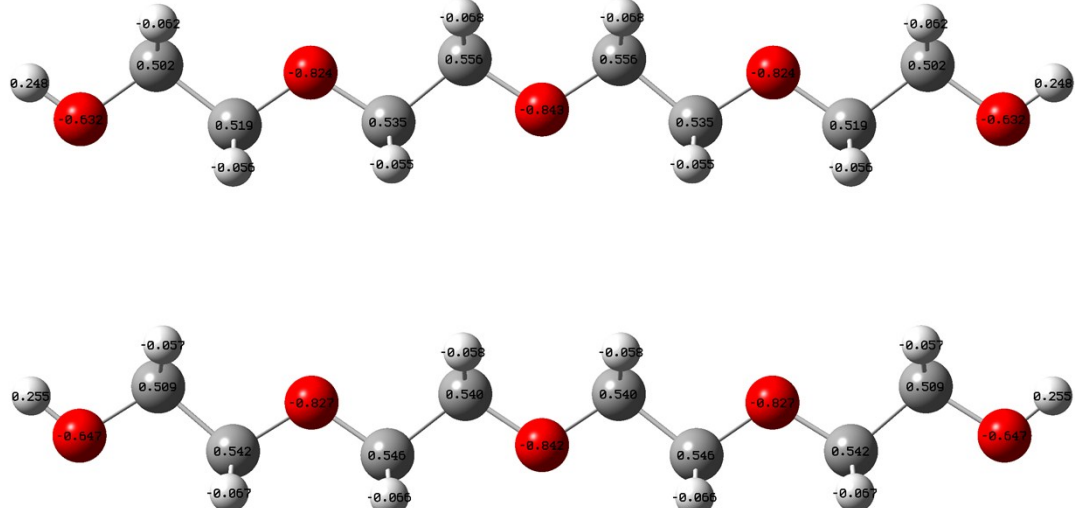


Figure S20. Charge distribution of PEG200-PEG200.

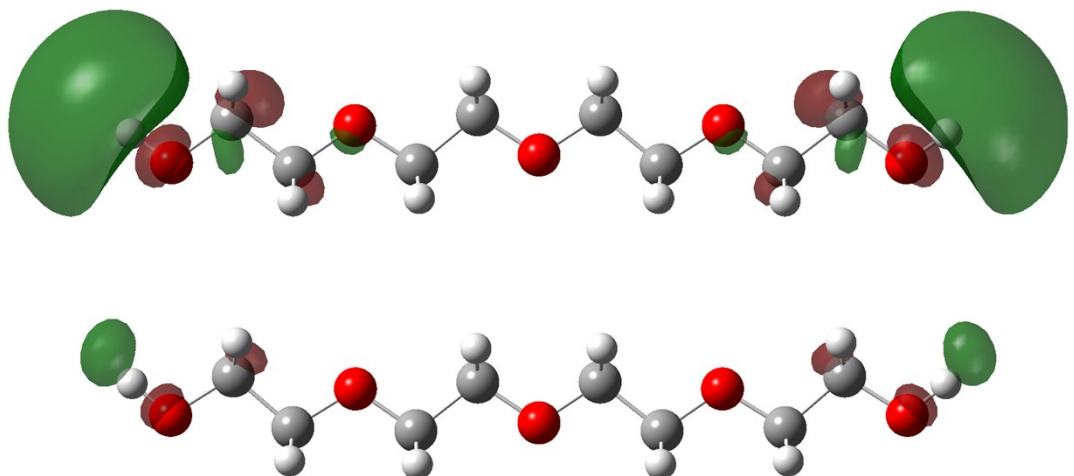


Figure S21. LUMO energy of PEG200-PEG200.

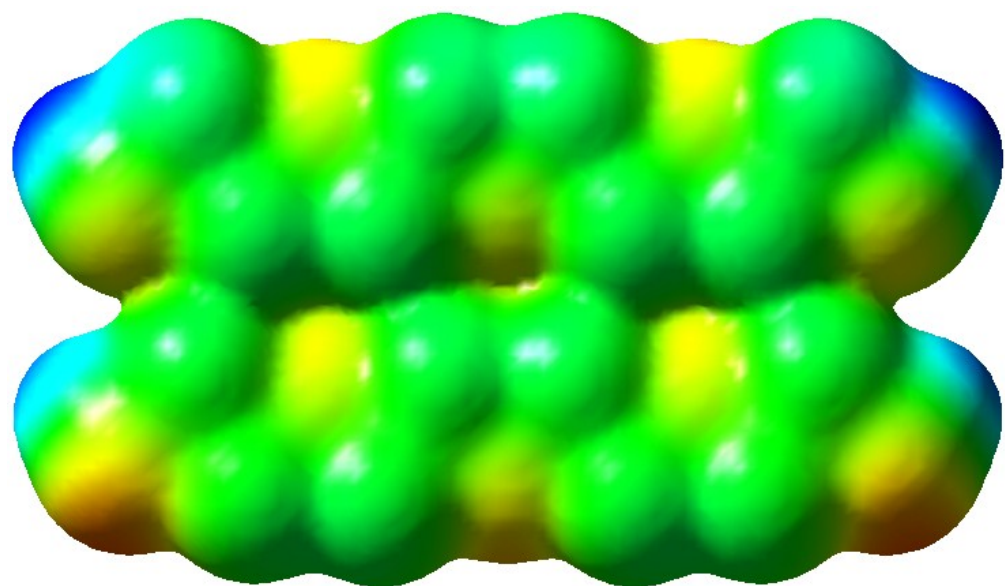


Figure S22. ESP of PEG200-PEG200.

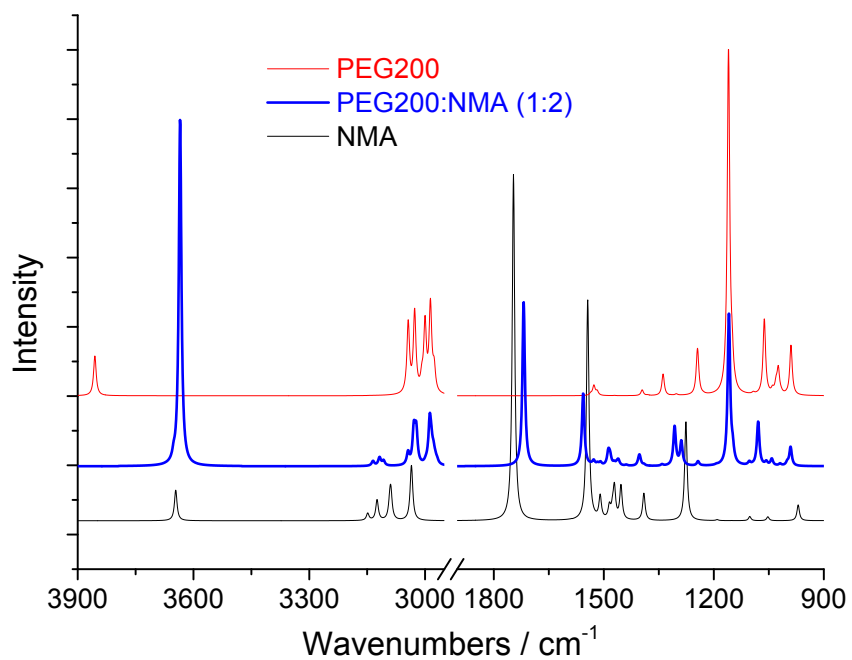


Figure S23. Simulated IR spectra of PEG200, NMA and PEG200:NMA (1:2).

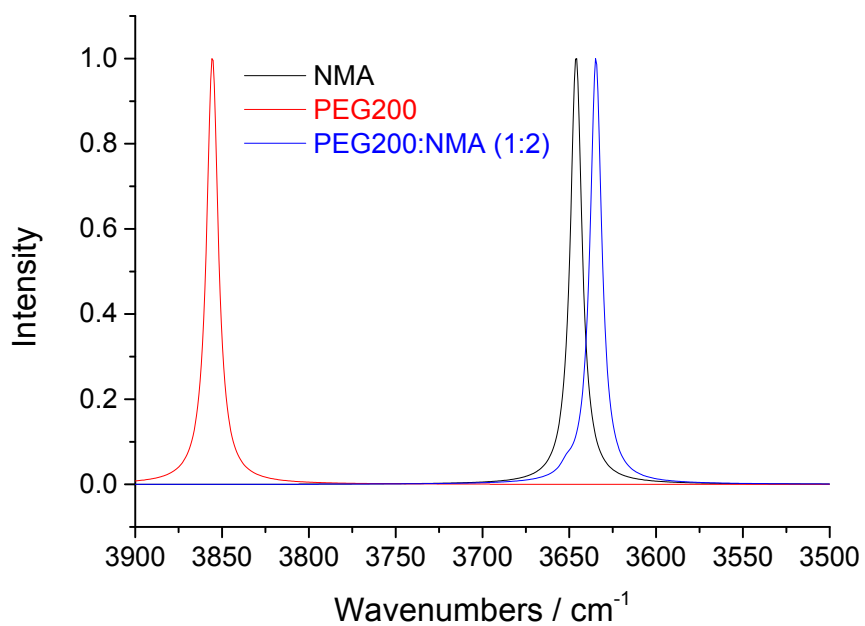


Figure S24. Simulated normalized IR spectra of PEG200, NMA and PEG200:NMA (1:2) in the wavenumber range of 3900~3500 cm⁻¹.

Table S7. Simulated IR peak and intensity of PEG200, NMA and PEG200:NMA (1:2).

	Peak of PEG200 / cm ⁻¹	Intensity		Peak of NMA / cm ⁻¹	Intensity		Peak of PEG200:NMA (1:2) / cm ⁻¹	Intensity
1	874.9	5.1	1	829.8	0.0	1	828.2	0.0
2	970.0	13.8	2	834.1	0.4	2	831.3	1.9
3	1052.7	3.4	3	840.3	0.0	3	838.1	0.0
4	1102.0	3.7	4	846.1	0.6	4	845.4	1.1
5	1151.1	0.1	5	989.6	109.1	5	880.1	9.5
6	1190.9	0.8	6	1016.5	2.9	6	880.2	0.2
7	1276.2	86.3	7	1024.2	54.4	7	990.7	104.4
8	1390.8	23.5	8	1030.2	21.5	8	999.6	7.7
9	1453.3	29.4	9	1039.9	10.0	9	999.7	9.5
10	1471.3	27.4	10	1062.2	156.5	10	1019.3	10.4
11	1476.4	7.8	11	1064.1	10.3	11	1040.8	4.4
12	1484.9	10.9	12	1092.3	3.4	12	1042.1	33.3
13	1510.0	19.9	13	1142.3	2.6	13	1055.9	6.8
14	1544.1	191.9	14	1142.6	0.0	14	1057.4	0.5
15	1746.5	300.6	15	1150.0	53.4	15	1057.4	13.5
16	3033.9	4.8	16	1150.7	0.0	16	1079.1	228.2
17	3035.4	43.8	17	1159.6	0.6	17	1080.5	16.4
18	3088.6	22.3	18	1160.0	753.1	18	1093.9	1.0
19	3091.4	12.2	19	1162.1	0.0	19	1093.9	1.1
20	3124.4	17.8	20	1173.6	0.0	20	1103.2	17.9
21	3148.6	6.2	21	1223.6	0.0	21	1142.6	0.0
22	3646.1	26.7	22	1228.8	0.9	22	1143.0	1.8
			23	1236.9	0.0	23	1143.2	0.1
			24	1243.6	24.9	24	1148.4	0.9
			25	1244.4	55.4	25	1148.6	67.6
			26	1245.6	24.6	26	1151.4	0.0
			27	1297.4	0.0	27	1157.8	0.2
			28	1298.3	0.0	28	1158.9	832.0
			29	1302.4	2.6	29	1162.8	0.3
			30	1302.4	0.0	30	1173.9	0.0
			31	1338.4	47.3	31	1192.6	1.5
			32	1357.6	0.0	32	1192.6	1.6
			33	1380.6	1.2	33	1223.3	0.0
			34	1395.5	12.5	34	1228.9	0.7
			35	1433.0	0.1	35	1236.8	0.0
			36	1454.8	0.0	36	1243.1	24.5

			37	1470.5	0.5	37	1288.6	31.7
			38	1477.1	0.0	38	1288.7	100.4
			39	1511.3	0.2	39	1296.4	0.0
			40	1514.1	0.0	40	1297.2	0.1
			41	1518.2	8.8	41	1299.0	2.3
			42	1525.3	0.0	42	1299.0	0.0
			43	1527.1	21.6	43	1306.8	192.1
			44	1532.2	0.1	44	1308.3	27.1
			45	1534.7	0.2	45	1341.2	7.8
			46	1536.1	3.8	46	1362.9	0.2
			47	2973.2	0.0	47	1390.6	7.2
			48	2975.2	2.0	48	1402.3	44.0
			49	2976.4	48.2	49	1402.3	3.1
			50	2982.4	1.7	50	1404.7	20.6
			51	2984.2	1.5	51	1438.8	5.4
			52	2986.2	189.1	52	1459.5	10.6
			53	2999.9	9.5	53	1460.9	20.3
			54	3000.0	140.1	54	1464.3	10.3
			55	3000.1	0.0	55	1471.5	1.9
			56	3001.2	0.0	56	1471.5	11.7
			57	3008.4	0.1	57	1482.1	11.7
			58	3008.4	27.9	58	1482.9	29.0
			59	3027.0	176.5	59	1484.7	1.7
			60	3027.8	0.0	60	1485.1	15.8
			61	3043.6	0.2	61	1487.8	57.9
			62	3043.7	154.5	62	1488.3	9.8
			63	3855.6	77.5	63	1509.0	4.3
			64	3855.6	9.7	64	1509.1	11.1
					65	1510.6	1.3	
					66	1513.0	0.8	
					67	1517.4	11.2	
					68	1525.8	0.5	
					69	1527.8	25.3	
					70	1532.0	0.1	
					71	1534.3	0.9	
					72	1535.8	2.3	
					73	1556.4	25.9	
					74	1556.4	376.1	
					75	1718.7	822.1	
					76	1719.0	83.8	
					77	2968.6	17.1	
					78	2969.1	0.6	
					79	2973.6	25.5	
					80	2978.1	51.9	
					81	2978.9	11.3	
					82	2983.8	86.8	
					83	2987.7	23.8	
					84	2987.9	207.2	
					85	2995.5	5.0	

						86	2996.1	0.0
						87	2998.5	9.7
						88	2998.6	0.0
						89	3022.8	184.3
						90	3024.0	0.0
						91	3029.0	0.7
						92	3029.1	189.5
						93	3043.7	7.6
						94	3043.7	7.8
						95	3044.2	24.1
						96	3044.3	27.8
						97	3107.5	5.4
						98	3107.5	22.0
						99	3116.8	5.1
						100	3116.8	8.1
						101	3118.3	26.2
						102	3118.3	7.4
						103	3134.9	13.3
						104	3135.0	12.8
						105	3634.6	1809.0
						106	3635.3	105.4
						107	3651.5	17.7
						108	3651.5	18.7

References in Supporting Information:

- [1] H. Ghaedi, M. Ayoub, S. Sufian, A.M. Shariff, G. Murshid, S.M. Hailegiorgis, S.N. Khan, Density, excess and limiting properties of (water and deep eutectic solvent) systems at temperatures from 293.15 K to 343.15 K. *J. Mol. Liq.* 248 (2017) 378-390.
- [2] Y. Xie, H. Dong, S. Zhang, X. Lu, X. Ji, Effect of Water on the Density, Viscosity, and CO₂ Solubility in Choline Chloride/Urea. *J. Chem. Eng. Data* 59 (2015) 3344-3352.
- [3] N.-n. Ren, Y.-h. Gong, Y.-z. Lu, H. Meng, C.-x. Li, Surface Tension Measurements for Seven Imidazolium-Based Dialkylphosphate Ionic Liquids and Their Binary Mixtures with Water (Methanol or Ethanol) at 298.15 K and 1 atm. *J. Chem. Eng. Data* 59 (2014) 189-196.
- [4] Access Date: May 28, 2019.
- [5] T. Ban, X.-P. Li, C.-L. Li, Q. Wang, Measurements of the solubility parameter and enthalpies of vaporization in N-alkyl-pyridinium bis((trifluoromethyl)sulfonyl) imide [C_nPY][NTF₂], n=4,6,8) ionic liquid. *Fluid Phase Equilib.* 485 (2019) 94-100.
- [6] W. Guan, J. Tong, S.-P. Chen, Q.-S. Liu, S.-L. Gao, Density and Surface Tension of Amino Acid Ionic Liquid 1-Alkyl-3-methylimidazolium Glutamate. *J. Chem. Eng. Data* 55 (2010) 4075-4079.
- [7] M.S. Dionisio, J.J.M. Ramos, R.M. Goncalves, The enthalpy and entropy of cavity formation in liquids and corresponding states principle. *Can. J. Chem.* 68 (1990) 1937-1949.
- [8] K.A. Kurnia, M.I.A. Mutalib, Z. Man, M.A. Bustam, Density and Surface Tension of Ionic Liquids [H₂N-C₂mim][PF₆] and [H₂N-C₃mim][PF₆]. *J. Chem. Eng. Data* 57 (2012) 2923-2927.
- [9] Q.-S. Liu, J. Tong, Z.-C. Tan, U. Welz-Biermann, J.-Z. Yang, Density and Surface Tension of Ionic Liquid [C₂mim][PF₃(CF₂CF₃)₃] and Prediction of Properties [C_nmim][PF₃(CF₂CF₃)₃] (n=1, 3, 4, 5, 6). *J. Chem. Eng. Data* 55 (2010) 2586-2589.
- [10] G. Yu, X. Chen, C. Asumana, S. Zhang, X. Liu, G. Zhou, Vaporization Enthalpy and Cluster Species in Gas Phase of 1,1,3,3-Tetramethylguanidinium-Based Ionic Liquids from Computer Simulations. *AIChE J.* 57 (2011) 507-516.
- [11] R. Ludwig, U. Kragl, Do we understand the volatility of ionic liquids? *Angew. Chem. Int. Ed.* 46 (2007) 6582-6584.
- [12] D.H. Zaitsau, V.N. Emel'yanenko, P. Stange, C. Schick, S.P. Verevkin, R. Ludwig, Dispersion and Hydrogen Bonding Rule: Why the Vaporization Enthalpies of Aprotic Ionic Liquids Are Significantly

Larger than those of Protic Ionic liquids. *Angew. Chem. Int. Ed.* 55 (2016) 11682-11686.

- [13] F. Heym, W. Korth, J. Thiessen, C. Kern, A. Jess, Evaporation and Decomposition Behavior of Pure and Supported Ionic Liquids under Thermal Stress. *Chem. Ing. Tech.* 87 (2015) 791-802.
- [14] D.H. Zaitsau, K. Fumino, V.N. Emel'yanenko, A.V. Yermalayeu, R. Ludwig, S.P. Verevkin, Structure-Property Relationships in Ionic Liquids: A Study of the Anion Dependence in Vaporization Enthalpies of Imidazolium-Based Ionic Liquids. *ChemPhysChem* 13 (2012) 1868-1876.
- [15] F.M.S. Ribeiro, C.F.R.A.C. Lima, I.C.M. Vaz, A.S.M.C. Rodrigues, E. Sapei, A. Melo, A.M.S. Silva, L.M.N.B.F. Santos, Vaporization of protic ionic liquids derived from organic superbases and short carboxylic acids. *Phys. Chem. Chem. Phys.* 19 (2017) 16693-16701.
- [16] D.H. Zaitsau, A.V. Yermalayeu, V.N. Emel'yanenko, S.P. Verevkin, U. Welz-Biermann, T. Schubert, Structure-property relationships in ILs: A study of the alkyl chain length dependence in vaporisation enthalpies of pyridinium based ionic liquids. *Sci. China Chem.* 55 (2012) 1525-1531.
- [17] A.V. Yermalayeu, D.H. Zaitsau, M. Loor, J. Schaumann, V.N. Emel'yanenko, S. Schulz, S.P. Verevkin, Imidazolium Based Ionic Liquids: Impact of the Cation Symmetry and Alkyl Chain Length on the Enthalpy of Vaporization. *Z. Anorg. Allg. Chem.* 643 (2017) 81-86.
- [18] K. Wu, T. Su, D.M. Hao, W.P. Liao, Y.C. Zhao, W.Z. Ren, C.L. Deng, H.Y. Lu, Choline chloride-based deep eutectic solvents for efficient cycloaddition of CO₂ with propylene oxide. *Chem. Commun.* 54 (2018).
- [19] X. Zhao, X. Lan, D. Yu, H. Fu, Z. Liu, T. Mu, Deep eutectic-solvothermal synthesis of nanostructured Fe₃S₄ for electrochemical N₂ fixation under ambient conditions. *Chem. Commun.* 54 (2018) 13010-13013.
- [20] K. Mukherjee, E. Tarif, A. Barman, R. Biswas, Dynamics of a PEG based non-ionic deep eutectic solvent: Temperature dependence. *Fluid Phase Equilib.* 448 (2017) 22-29.
- [21] R.-L. Liu, P. Yu, X.-L. Ge, X.-F. Bai, X.-Q. Li, Q. Fu, Establishment of an Aqueous PEG 200-Based Deep Eutectic Solvent Extraction and Enrichment Method for Pumpkin (*Cucurbita moschata*) Seed Protein. *Food Anal. Method.* 10 (2017) 1669-1680.
- [22] J. Jiang, C. Yan, X. Zhao, H. Luo, Z. Xue, T. Mu, A PEGylated deep eutectic solvent for controllable solvothermal synthesis of porous NiCo₂S₄ for efficient oxygen evolution reaction. *Green Chem.* 19 (2017) 3023-3031.
- [23] C. Li, J. Zhang, Z. Li, J. Yin, Y. Cui, Y. Liu, G. Yang, Extraction desulfurization of fuels with

- 'metal ions' based deep eutectic solvents (MDESS). *Green Chem.* 18 (2016) 3789-3795.
- [24] W. Chen, X. Bai, Z. Xue, H. Mou, J. Chen, Z. Liu, T. Mu, The formation and physicochemical properties of PEGylated deep eutectic solvents. *New J. Chem.* 43 (2019) 8804-8810.
- [25] Y. Zhang, X. Ji, X. Lu, Choline-based deep eutectic solvents for CO₂ separation: Review and thermodynamic analysis. *Renew. Sustain. Energy Rev.* 97 (2018) 436-455.
- [26] H. Zhang, Y. Wang, Y. Zhou, K. Xu, N. Li, Q. Wen, Q. Yang, Aqueous biphasic systems containing PEG-based deep eutectic solvents for high-performance partitioning of RNA. *Talanta* 170 (2017) 266-274.